

# River pollution problem in the advection dominated case

**Student:** Paolo GIARETTA

## 1 Problem description

This project aims to investigate the numerical stability of the Finite Element Method in the *advection-dominated* case. In particular, the straightforward Galerkin discretization of the relevant PDE will be compared with schemes employing SUPG stabilization.

The problem under interest is that of a factory that spills pollutants in a river. The computational domain of the river is modeled as a rectangular region  $\Omega = [0, L] \times [0, W]$  in the  $xy$  plane of length  $L$  and width  $W$  (Fig.1). The problem can be treated as 2D as we assume the pollution does not involve the underwater layers of the river.

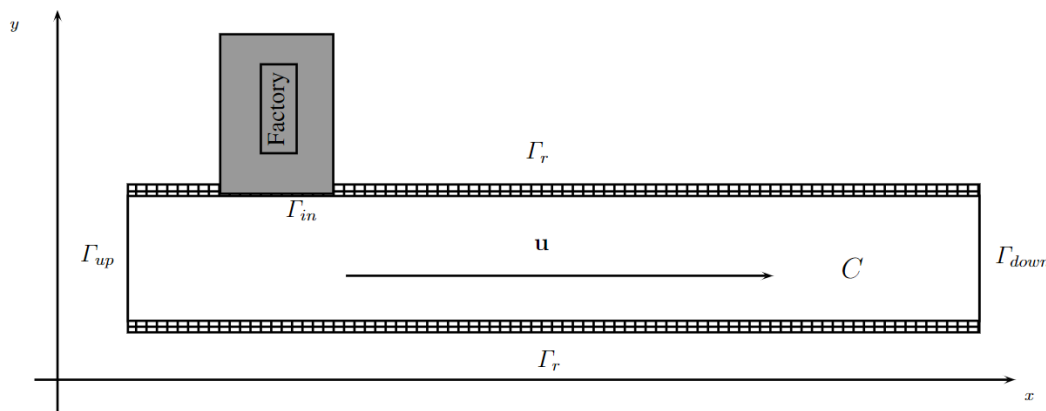


Figure 1: Computational domain of the problem.

All the assumptions that lead to the final PDE are:

- The concentration at the factory's inlet  $\Gamma_{in} = \{(x, W), F_{start}^{in} \leq x \leq F_{end}^{in}\}$  is fixed at  $C_{in}$ .
- In correspondence of the upstream boundary  $\Gamma_{up}$  there is a small baseline concentration  $C_{up}$ .
- The downstream section  $\Gamma_{down}$  is far enough that the concentration no longer changes in the direction of the flux normal to the boundary.
- The flux of pollutants on the river sides is proportional to the difference in concentration between the natural concentration in the soil  $C_{dry}$  and the river concentration, where  $\alpha$  denotes the proportionality constant.
- The diffusivity of the pollutant in the river is isotropic, so it is represented by the proportionality constant  $\mu$ .
- The water velocity field  $\mathbf{u}$  is steady and divergence-free.
- Bacterium in the river reacts with the pollutant with first-order kinetics, thus the pollutant decays with rate  $\sigma$ .
- The whole problem is steady, thus there is no change in time.

Under these assumptions, the problem can be described by the following PDE (1), where  $C$  denotes the steady pollutant concentration.

$$\begin{cases} -\mu\Delta C + \mathbf{u} \cdot \nabla u + \sigma u = 0, & \text{in } \Omega \\ C = C_{in}, & \text{on } \Gamma_{in} \\ C = C_{up}, & \text{on } \Gamma_{up} \\ \mu\partial_n C = 0, & \text{on } \Gamma_{down} \\ \mu\partial_n C = \alpha(C_{dry} - C), & \text{on } \Gamma_r = \partial\Omega \setminus (\Gamma_{in} \cup \Gamma_{up} \cup \Gamma_{down}) \end{cases} \quad (1)$$

The values of the parameters employed for all numerical solutions are:

Parameter	Value
River width	$W = 2$
River length	$L = 10$
Factory positions	$F_{start}^{in} = 1, F_{end}^{in} = 3$
Baseline upstream concentration	$C_{up} = 1g/m^3$
Dry soil concentration	$C_{dry} = 1g/m^3$
Soil absorption constant	$\alpha = 0.1$
Pollutant diffusivity	$\mu = 10^{-6}$
Decay rate	$\sigma = 0.5$
Centerline velocity	$u_M = 10$

Table 1: Parameters

The factory inlet concentration profile is (Fig.2):

$$C_{in} = C_{up} + 15 [1 - \cos(\pi(x - 1))] g/m^3 \quad (2)$$

The upstream velocity profile is parabolic (Fig.2) and given by:

$$\mathbf{u} = [u_1, u_2] = [u_M(W - y)y, 0] m/s \quad (3)$$

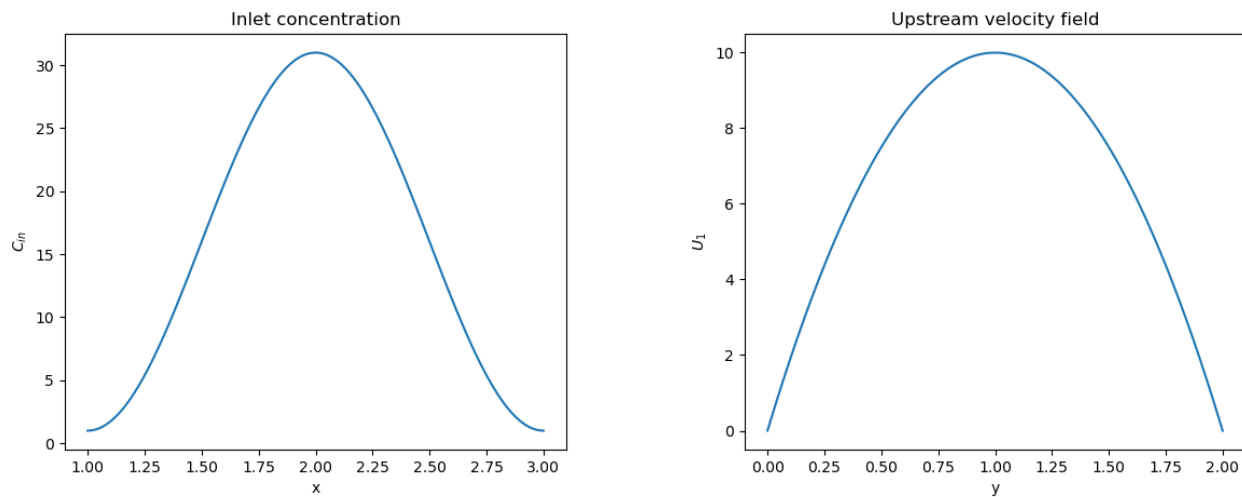


Figure 2: Inlet concentration and upstream velocity profiles.

## 2 Solution

### 2.1 Well-posedness of the PDE

Before discretizing the PDE for the Finite Element Method, we study the well-posedness of the PDE. First, it is necessary to rewrite the corresponding weak form of (1) by multiplying the left side by a generic test function  $\phi$  and integrating it over  $\Omega$ .

$$-\mu \int_{\Omega} \Delta C \phi + \int_{\Omega} \mathbf{u} \cdot \nabla C \phi + \sigma \int_{\Omega} C \phi = 0 \quad (4)$$

By using the vector identities and the divergence theorem we can rewrite the integrals as follows:

$$-\mu \int_{\Omega} \Delta C \Delta \phi = \mu \int_{\Omega} \nabla C \cdot \nabla \phi - \mu \int_{\partial\Omega} \partial_n C \phi \quad (5)$$

$$\begin{aligned} \mu \int_{\partial\Omega} \partial_n C \phi &= \mu \int_{\Gamma_{down}} \underbrace{\partial_n C}_{=0} \phi + \mu \int_{\Gamma_{up} \cup \Gamma_{in}} \partial_n C \phi + \mu \int_{\Gamma_r} \partial_n C \phi = \mu \int_{\Gamma_{up}} \partial_n C \phi + \mu \int_{\Gamma_{in}} \partial_n C \phi + \int_{\Gamma_r} \alpha(C_{dry} - C) \phi \end{aligned} \quad (6)$$

Thus, the weak formulation becomes:

$$\mu \int_{\Omega} \nabla C \cdot \nabla \phi + \int_{\Omega} \mathbf{u} \cdot \nabla C \phi + \sigma \int_{\Omega} C \phi + \alpha \int_{\Gamma_r} C \phi = \mu \int_{\Gamma_{up}} \partial_n C \phi + \mu \int_{\Gamma_{in}} \partial_n C \phi + \alpha C_{dry} \int_{\Gamma_r} \phi \quad (7)$$

To apply the Max-Milgram Lemma we have to specify in which Hilbert space the functions  $u$  and  $\phi$  live. Given the inhomogeneous Dirichlet boundary conditions, we can write  $C = C_0 + C_{\Gamma}$ . Where  $C_0 \in H_0^1(\Omega)$  and  $C_{\Gamma} \in H^1(\Omega)$  such that  $\gamma_{\Gamma_{up}}(C_{\Gamma}) = C_{up}$ ,  $\gamma_{\Gamma_{in}}(C_{\Gamma}) = C_{in}$ . By requiring that both  $C_0$  and  $\phi$  belong to the Sobolev space  $H_0^1(\Omega)$  the following terms vanish from the right-hand side.

$$\mu \int_{\Gamma_{up}} \partial_n C \phi = \mu \int_{\Gamma_{in}} \partial_n C \phi = 0 \quad (8)$$

Moreover, by substituting  $C = C_0 + C_{\Gamma}$  into (9), we can properly formulate the weak problem as:

$$\mu \int_{\Omega} \nabla C_0 \cdot \nabla \phi + \int_{\Omega} \mathbf{u} \cdot \nabla C_0 \phi + \sigma \int_{\Omega} C_0 \phi + \alpha \int_{\Gamma_r} C_0 \phi = \alpha C_{dry} \int_{\Gamma_r} \phi + f_{Dir}(C_{\Gamma}, \phi), \quad \forall \phi \in H_0^1(\Omega) \quad (9)$$

Where  $f_{Dir}(C_{\Gamma}, \phi)$  is the right-hand side contribution due to the inhomogeneous Dirichlet conditions. In the numerical scheme, the Dirichlet conditions will be imposed by fixing the solution on the boundary. For simplicity, I will neglect the presence of this term in the proof of well-posedness.

In the formalism of the Max-Milgram lemma, the problem can be rephrased in terms of the bilinear form  $a(u, v)$  and right-hand side functional  $f(v)$ :

$$a(u, v) = f(v) \quad \forall v \in H_0^1(\Omega) \quad \text{and} \quad u \in H_0^1(\Omega) \quad (10)$$

$$a(u, v) = \mu \int_{\Omega} \nabla u \cdot \nabla v + \int_{\Omega} \mathbf{u} \cdot \nabla u v + \sigma \int_{\Omega} u v + \alpha \int_{\Gamma_r} u v \quad (11)$$

$$f(v) = \alpha C_{dry} \int_{\Gamma_r} v \quad (12)$$

The existence and uniqueness of the solution are guaranteed by the Max-Milgram lemma. To apply the lemma, it is necessary to prove the continuity of both forms and coercitivity of  $a$  inside the Hilbert space  $H_0^1(\Omega)$ .

#### Continuity

Continuity of the forms  $a$  and  $f$  in the Hilbert space  $H_0^1(\Omega)$  corresponds to the existence of constants  $M$  and  $M'$  such that:

$$|a(u, v)| \leq M \|u\|_{H^1(\Omega)} \|v\|_{H^1(\Omega)}, \quad \forall u, v \in H_0^1(\Omega) \quad (13)$$

$$|f(v)| \leq M' \|v\|_{H^1(\Omega)}, \quad \forall v \in H_0^1(\Omega) \quad (14)$$

By applying Cauchy-Schwarz and  $\|u\|_{H^1(\Omega)}^2 = \|u\|_{L^2(\Omega)}^2 + \|\nabla u\|_{L^2(\Omega)}^2 \geq \max\{\|u\|_{L^2(\Omega)}^2, \|\nabla u\|_{L^2(\Omega)}^2\}$  we have the following bounds:

$$\mu \left| \int_{\Omega} \nabla u \cdot \nabla v \right| \leq \mu \|\nabla u\|_{L^2(\Omega)} \|\nabla v\|_{L^2(\Omega)} \leq \mu \|u\|_{H^1(\Omega)} \|v\|_{H^1(\Omega)} \quad (15)$$

$$\sigma \left| \int_{\Omega} uv \right| \leq \sigma \|u\|_{L^2(\Omega)} \|v\|_{L^2(\Omega)} \leq \sigma \|u\|_{H^1(\Omega)} \|v\|_{H^1(\Omega)} \quad (16)$$

The transport term can be bounded as follows, where  $|\mathbf{u}|_{L^\infty(\Omega)} = \text{supess}_{x \in \Omega} |\mathbf{u}| = u_M W^2 / 4$ :

$$\left| \int_{\Omega} \mathbf{u} \cdot \nabla u v \right| \leq \int_{\Omega} |\mathbf{u}| |\nabla u| |v| \leq |\mathbf{u}|_{L^\infty(\Omega)} \|\nabla u\|_{L^2(\Omega)} \|v\|_{L^2(\Omega)} \leq |\mathbf{u}|_{L^\infty(\Omega)} \|u\|_{H^1(\Omega)} \|v\|_{H^1(\Omega)} \quad (17)$$

To bound the integral terms over  $\Gamma_r$  we can resolve to the trace inequality, i.e  $\exists C_T : \|\gamma(v)\|_{L^2(\Gamma_r)} \leq C_T \|v\|_{H^1(\Omega)}$ :

$$\alpha \left| \int_{\Gamma_r} uv \right| \leq \alpha \|u\|_{L^2(\Gamma_r)} \|v\|_{L^2(\Gamma_r)} \leq \alpha C_T^2 \|u\|_{H^1(\Omega)} \|v\|_{H^1(\Omega)} \quad (18)$$

$$\alpha C_{dry} \left| \int_{\Gamma_r} v \right| \leq \alpha C_{dry} \sqrt{|\Gamma_r|} \|v\|_{L^2(\Gamma_r)} \leq \alpha C_{dry} \sqrt{|\Gamma_r|} C_T \|v\|_{H^1(\Omega)} \quad (19)$$

Putting all boundings together, we obtain the continuity of forms  $a$  and  $f$ . Similarly, we can bound all additional terms present in  $f_{Dir}(C_\Gamma, \phi)$ .

### Coercitivity

Coercitivity of the bilinear form  $a$  signifies that there exists a constant  $\alpha > 0$  such that  $a(u, u) \geq \alpha \|u\|_{H_0^1(\Omega)}^2$ ,  $\forall u \in H_0^1(\Omega)$ . Indeed:

$$\begin{aligned} a(u, u) &= \mu \int_{\Omega} |\nabla u|^2 + \int_{\Omega} \mathbf{u} \cdot \nabla u u + \sigma \int_{\Omega} u^2 + \alpha \int_{\Gamma_r} u^2 \\ &\geq \mu \int_{\Omega} |\nabla u|^2 + \sigma \int_{\Omega} u^2 + \frac{1}{2} \int_{\Omega} \mathbf{u} \cdot \nabla u^2 \\ &= \mu \int_{\Omega} |\nabla u|^2 + \sigma \int_{\Omega} u^2 - \frac{1}{2} \int_{\Omega} \underbrace{(\nabla \cdot \mathbf{u}) u^2}_{=0} + \frac{1}{2} \int_{\partial\Omega} \underbrace{(\mathbf{u} \cdot \mathbf{n}) u^2}_{=0} \\ &\geq \underbrace{\min\{\mu, \sigma\}}_{=\alpha} \int_{\Omega} u^2 + |\nabla u|^2 = \alpha \|u\|_{H_0^1(\Omega)}^2 \end{aligned} \quad (20)$$

## 2.2 Domain discretization

The continuous rectangular domain has been discretized into a triangular mesh refined around the boundaries and the factory inlet. The mesh is controlled by three parameters  $h$ ,  $h_b$ ,  $h_f$  denoting the target mesh diameters in the domain  $\Omega$ , the boundary  $\Gamma = \partial\Omega \setminus \Gamma_{in}$  and the factory inlet  $\Gamma_{in}$ . To smooth the transition between the different mesh sizes, the target mesh size at any point  $(x, y) \in \Omega$  is calculated from the

distance from the boundary and factory inlet. The mesh changes as a function of the distances following two Gaussians with standard deviations  $\sigma_b$ , and  $\sigma_f$  respectively (21).

$$h(x, y) = h + \min\{(h_b - h) \exp\left(-\frac{d_b(x, y)^2}{2\sigma_b^2}\right), (h_f - h) \exp\left(-\frac{d_f(x, y)^2}{2\sigma_f^2}\right)\} \quad (21)$$

Where  $d_b(x, y)$ ,  $d_f(x, y)$  denote the distances of point  $(x, y)$  from the boundary and factory inlet respectively. An example of so-obtained mesh is reported in Fig.3.

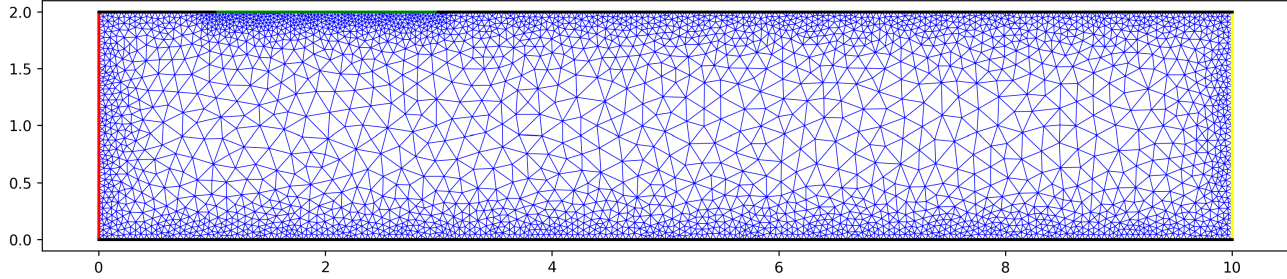


Figure 3: Mesh for  $h = 0.2$ ,  $h_b = 0.05$ ,  $h_f = 0.03$ ,  $\sigma_b = 0.3$ ,  $\sigma_f = 0.3$ .

### 2.3 Garlekin discretization

The problem is discretized using linear elements over the grid  $\tau_h$  to obtain the discrete concentration solution  $C_h$ . By introducing the basis functions  $\phi_v$ ,  $\forall v \in \tau_h$ , the discrete Garlekin problem derived from (9) becomes:

$$C_h = \sum_{j=1}^{|\tau_h|} C_h^j \phi_{v_j} \quad (22)$$

$$\sum_{j=1}^{|\tau_h|} \left( \underbrace{\mu \int_{\Omega} \nabla \phi_{v_j} \cdot \nabla \phi_{v_i}}_{\text{stiffness matrix}} + \underbrace{\int_{\Omega} \mathbf{u} \cdot \nabla \phi_{v_j} \phi_{v_i}}_{\text{transport matrix}} + \underbrace{\sigma \int_{\Omega} \phi_{v_j} \phi_{v_i} + \alpha \int_{\Gamma_r} \phi_{v_j} \phi_{v_i}}_{\text{mass matrix}} \right) C_h^j = \underbrace{\alpha C_{dry} \int_{\Gamma_r} \phi_{v_i}}_{\text{rhs}}, \quad \forall i = 1, \dots, |\tau_h| \quad (23)$$

The matrix components are calculated by splitting the integrals over each element, reformulating them on the reference triangle  $\hat{K}$ , and using numerical quadrature to approximate the integrals.

$$\int_{\Omega} \nabla \phi_{v_i} \cdot \nabla \phi_{v_j} = \sum_{K \in \tau_h} \int_K \nabla \phi_{v_i} \cdot \nabla \phi_{v_j} = \sum_{K \in \tau_h} \det B_K \int_{\hat{K}} (B_K^{-T} \hat{\nabla} \hat{\phi}_{v_i}) \cdot (B_K^{-T} \hat{\nabla} \hat{\phi}_{v_j}) \quad (24)$$

$$\int_{\Omega} \mathbf{u} \cdot \nabla \phi_{v_j} \phi_{v_i} = \sum_{K \in \tau_h} \int_K \mathbf{u} \cdot \nabla \phi_{v_j} \phi_{v_i} = \sum_{K \in \tau_h} \det B_K \int_{\hat{K}} \mathbf{u} \cdot (B_K^{-T} \hat{\nabla} \hat{\phi}_{v_j}) \hat{\phi}_{v_i} \quad (25)$$

$$\begin{aligned} \sigma \int_{\Omega} \phi_{v_j} \phi_{v_i} + \alpha \int_{\Gamma_r} \phi_{v_j} \phi_{v_i} &= \sum_{K \in \tau_h} \sigma \int_K \phi_{v_i} \phi_{v_j} + \sum_{(v_m, v_n) \in \Gamma_r} \alpha \int_{(v_m, v_n)} \phi_{v_i} \phi_{v_j} = \\ &= \sum_{K \in \tau_h} \sigma \det B_K \int_{\hat{K}} \hat{\phi}_{v_i} \hat{\phi}_{v_j} + \sum_{(v_m, v_n) \in \Gamma_r} \alpha |v_m - v_n| \frac{\delta_{im} \delta_{jn} + \delta_{in} \delta_{jm} + \delta_{im} \delta_{jm} + \delta_{in} \delta_{jn}}{6} \end{aligned} \quad (26)$$

$$\alpha C_{dry} \int_{\Gamma_r} \phi_{v_i} = \alpha C_{dry} \sum_{(v_m, v_n) \in \Gamma_r} \int_{(v_m, v_n)} \phi_{v_i} = \alpha C_{dry} \sum_{(v_m, v_n) \in \Gamma_r} |v_m - v_n| \frac{\delta_{im} + \delta_{in}}{2} \quad (27)$$

Where  $B_K$  is the linear transformation of the affine map between the reference triangle  $\hat{K}$ , and  $K$ .

## 2.4 No stabilization

The solution of the discrete problem without any numerical stabilization is reported in Fig.4 and Fig.5, for mesh parameters  $h = 0.2$ ,  $h_b = 0.025$ ,  $h_f = 0.01$ ,  $\sigma_b = 0.3$ ,  $\sigma_f = 0.3$ .

The solution is non-physical as the concentration reaches negative values. Moreover, the concentration profile near the inlet does not vary continuously as it is possible to observe large oscillations between neighboring elements. The presence of numerical oscillations is to be expected for solutions in which advection dominates over diffusion and without additional stabilization techniques. This is supported by the local Péclet number  $Pe = \frac{\|u\| h_K}{2\mu}$  as it reaches a maximum near the centerline of  $Pe_{max} \sim 10^6$ .

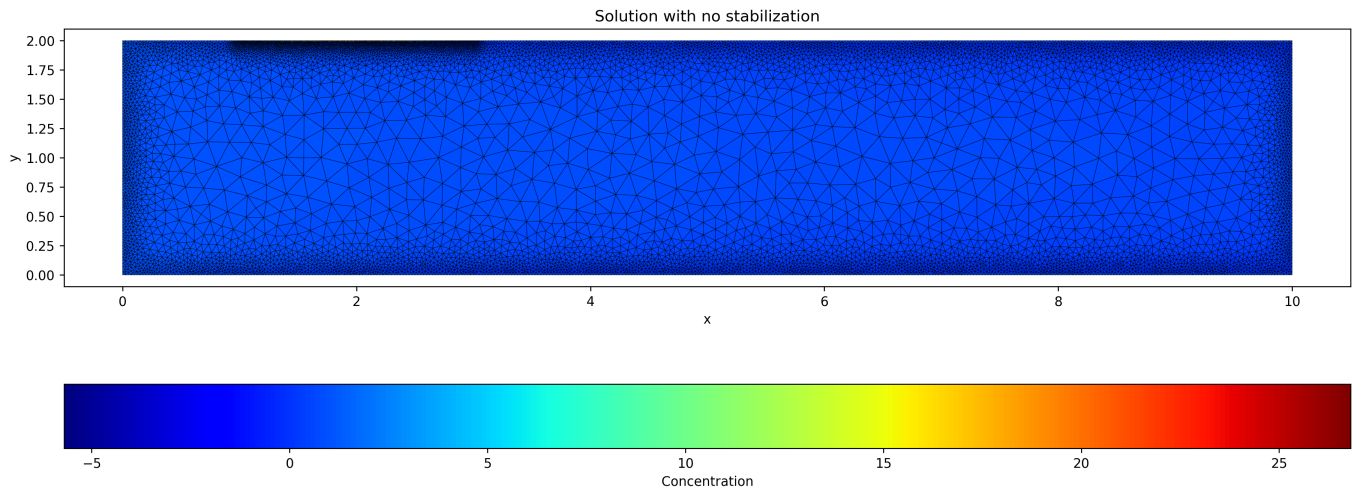


Figure 4: Concentration profile obtained with no stabilization.

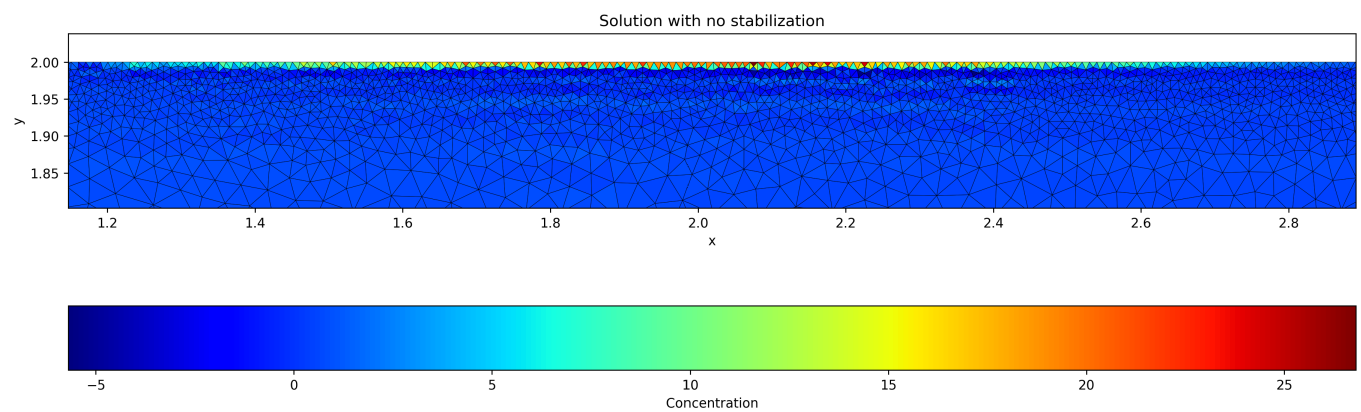


Figure 5: Zoom-in near the factory inlet.

## 2.5 SUPG stabilization

To avoid numerical instabilities, we can employ SUPG stabilization for the problem  $a(u, v) = f(v)$ . We modify the bilinear form and right-hand side by adding streamline diffusion as:

$$a_h(u, v) = a(u, v) + \sum_{K \in \tau_h} \gamma \frac{h_K}{\|\mathbf{u}\|} \int_K (\mathbf{u} \cdot \nabla v) (\mathbf{u} \cdot \nabla u + \sigma u) \quad (28)$$

$$R_h(v) = \int_{\Omega} f v + \sum_{K \in \tau_h} \gamma \frac{h_K}{\|\mathbf{u}\|} \int_K f (\mathbf{u} \cdot \nabla v) \text{ (+ additional boundary terms)} \quad (29)$$

Where  $\gamma$  is the stabilization parameter that determines the strength of the artificial diffusion. After applying Galerkin discretization, we have the additional SUPG terms:

$$\begin{aligned} a_{ij}^{SUPG} &= \sum_{K \in \tau_h} \gamma \frac{h_K}{\|\mathbf{u}\|} \int_K (\mathbf{u} \cdot \nabla \phi_{v_i}) (\mathbf{u} \cdot \nabla \phi_{v_j} + \sigma \phi_{v_j}) \\ &= \sum_{K \in \tau_h} \gamma \frac{h_K}{\|\mathbf{u}\|} \det B_K \int_{\hat{K}} (\mathbf{u} \cdot B_K^{-T} \hat{\nabla} \phi_{v_i}) (\mathbf{u} \cdot B_K^{-T} \hat{\nabla} \phi_{v_j} + \sigma \hat{\phi}_{v_j}) \end{aligned} \quad (30)$$

$$r_i^{SUPG} = \sum_{K \in \tau_h} \gamma \frac{h_K}{\|\mathbf{u}\|} \int_K f (\mathbf{u} \cdot \nabla \phi_{v_i}) = \sum_{K \in \tau_h} \gamma \frac{h_K}{\|\mathbf{u}\|} \det B_K \int_{\hat{K}} f (\mathbf{u} \cdot B_K^{-T} \hat{\nabla} \phi_{v_i}) \quad (31)$$

The numerical solution with SUPG stabilization for the same mesh parameters  $h = 0.2$ ,  $h_b = 0.025$ ,  $h_f = 0.01$ ,  $\sigma_b = 0.3$ ,  $\sigma_f = 0.3$  is reported in Fig.6 and Fig.7. A stabilization parameter  $\gamma = 5$  has been employed. As can be seen, the solution no longer presents numerical oscillations and it is possible to appreciate the effects of pollutant diffusion, advection, decay, and river absorption.

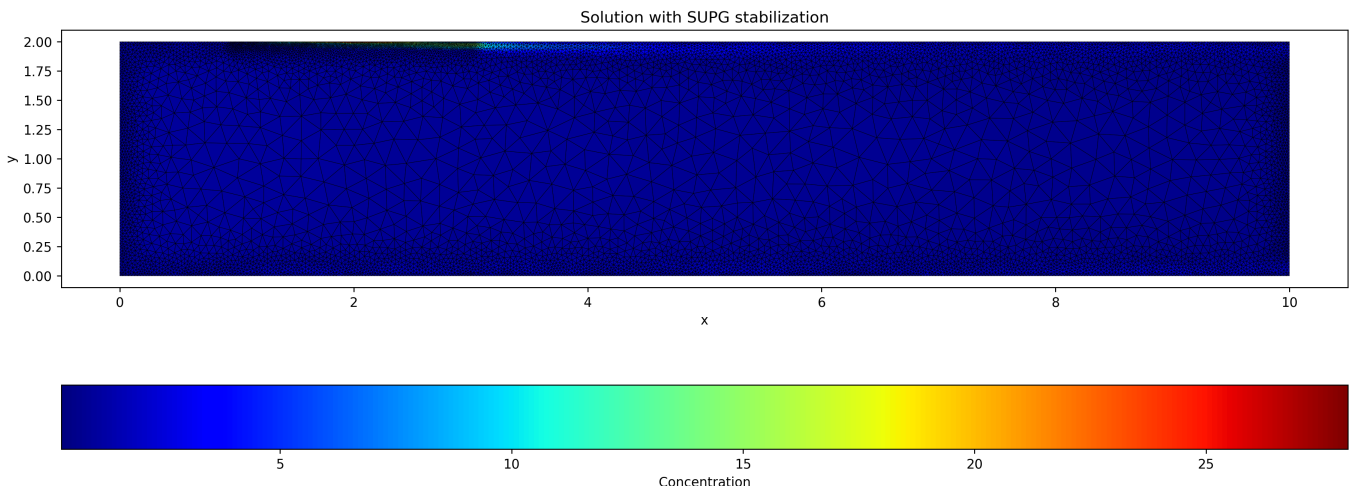


Figure 6: Numerical solution with SUPG stabilization for  $\gamma = 5$ .

## 2.6 Convergence

The convergence rate of the numerical scheme is based on the total pollutant quantity in  $\Omega$  at steady conditions (32).

$$Q = \int_{\Omega} C \approx \int_{\Omega} C_h = Q_h \quad (32)$$

The last integral can be calculated exactly from the Finite Element solution with linear elements as:

$$Q_h = \sum_{j=1}^{|\tau_h|} C_h^j \int_{\Omega} \phi_{v_j} = \sum_{j=1}^{|\tau_h|} C_h^j \sum_{K \in \tau_h: v_j \in K} \int_K \phi_{v_j} = \sum_{j=1}^{|\tau_h|} C_h^j \sum_{K \in \tau_h: v_j \in K} \frac{\det B_K}{6} = \sum_{(v_a, v_b, v_c) \in \tau_h} \det B_K \frac{C_h^a + C_h^b + C_h^c}{6} \quad (33)$$

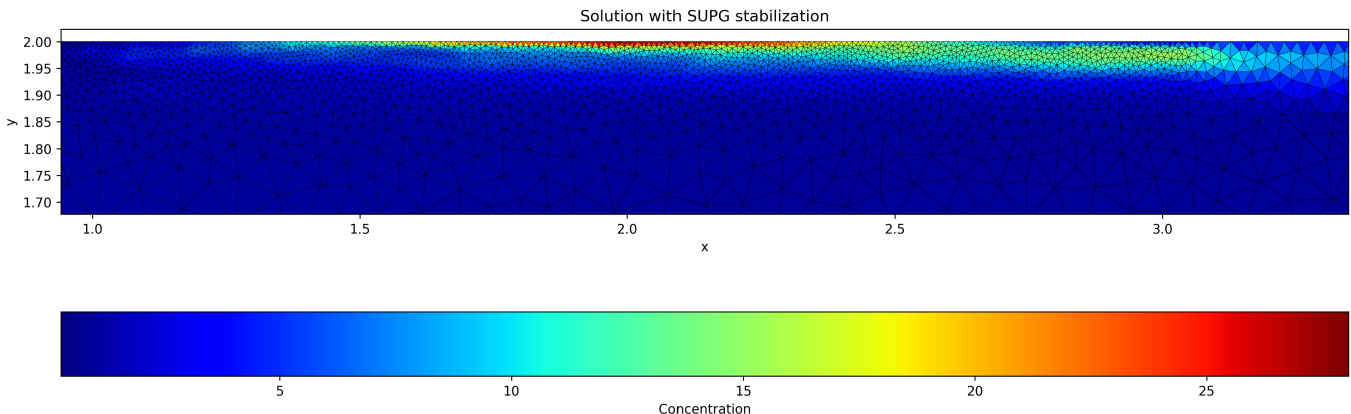


Figure 7: Zoom-in near the factory inlet.

The convergence rate can be estimated by calculating  $Q_h$  on a sufficiently refined grid  $\tau_{\tilde{h}}$  and studying the trend of the convergence error  $|Q_h - Q_{\tilde{h}}|$  against the grid parameter  $h$ . The convergence plot is reported in Fig.8 and in Table 2.

$h$	$h_b$	$h_f$	$Q_h$	$ Q_h - Q_{\tilde{h}} $
1.0000	0.1250	0.0500	17.5716	2.3259
0.9526	0.1191	0.0476	17.9763	1.9212
0.9053	0.1132	0.0453	18.0556	1.8419
0.8579	0.1072	0.0429	18.5105	1.3870
0.8105	0.1013	0.0405	17.8623	2.0352
0.7632	0.0954	0.0382	17.7162	2.1813
0.7158	0.0895	0.0358	17.5937	2.3038
0.6684	0.0836	0.0334	17.9890	1.9085
0.6211	0.0776	0.0311	17.6315	2.2660
0.5737	0.0717	0.0287	18.4741	1.4234
0.5263	0.0658	0.0263	17.8369	2.0606
0.4789	0.0599	0.0239	17.4729	2.4246
0.4316	0.0539	0.0216	18.1251	1.7724
0.3842	0.0480	0.0192	18.6910	1.2065
0.3368	0.0421	0.0168	18.2154	1.6821
0.2895	0.0362	0.0145	18.5426	1.3549
0.2421	0.0303	0.0121	18.9672	0.9303
0.1947	0.0243	0.0097	19.4341	0.4634
0.1474	0.0184	0.0074	19.3664	0.5311
0.1000	0.0125	0.0050	<b>19.8975</b>	-

Table 2: Convergence

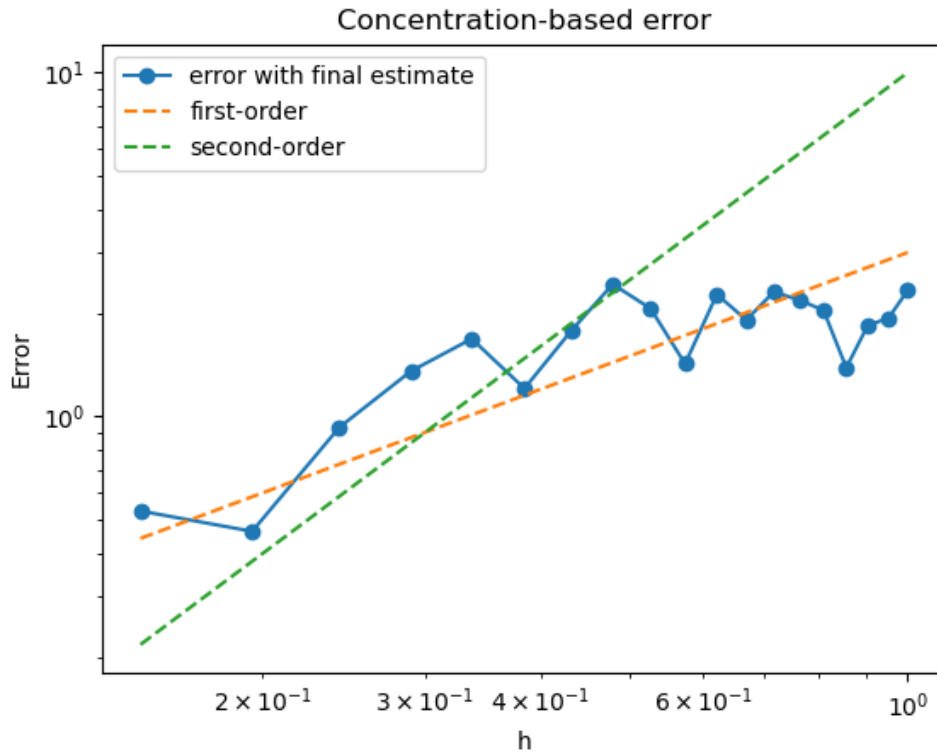


Figure 8: Error estimates as a function of  $h$  in the  $[0.1, 1]$  range.

The error reduces with diminishing mesh parameters  $h, h_b, h_f$ . The trend, however, is not perfectly consistent with either a first or second-order trend. This is likely due to the complex mesh geometry and relatively large element sizes to reach the asymptotic bounds. In the current implementation, values significantly smaller than  $h = 0.1, h_b = 0.0125, h_f = 0.0050$  become prohibitively expensive to run.

Assuming both the original and dual problems admit smooth solutions  $u, \phi \in H^2(\Omega)$  we expect the following error estimate:

$$|Q(u) - Q(u_h)| \leq Ch^2 |u|_{H^2(\Omega)} |\phi|_{H^2(\Omega)} \quad (34)$$

The smallest 4-5 points seem to follow more closely a second-order trend but it is not captured perfectly. It is expected that it becomes more consistent as the parameter  $h$  diminishes further.